Near-Field Pattern Synthesis for Sparse Focusing Antenna Arrays Based on Bayesian Compressive Sensing and Convex Optimization

Zi Xuan Huang, *Student Member, IEEE*, and Yu Jian Cheng, *Senior Member, IEEE*

***Abstract*— An effective method based on Bayesian compressive sensing (BCS) and convex optimization for near-field sparse array synthesis is presented in this paper. An algorithm to generate reference-shaped beams in the near-field region with controllable sidelobe levels is first proposed. Then, the multitask BC is modified and generalized to synthesize a near-field sparse array radiating a desired near-field pattern with the co-polarization component. After that, a postprocessing of the final array excitation is employed to put constraints on the minimum element spacing to make the sparse layout practicable. The degradation of the near-field pattern is mitigated through reestimating the array excitation by a convex optimization. Three numerical examples show the effectiveness of the proposed method with more than 50% of elements saved compared to the uniformly distributed layout. The comparison to the result obtained by a full-wave simulator FEKO is also presented to demonstrate the validity of this method considering strong antenna mutual couplings.**

***Index Terms*— Bayesian compressive sensing (BCS), convex optimization, near-field beam shaping, sparse array.**

I. Introduction

NEAR-FIELD focusing (NFF) array antennas have been applied in various areas both in industrial and biomedical applications [1]–[8], such as microwave imaging, remote sensing, wireless power transmission, RFIDs, hyperthermia, and so on.

Larger apertures are required for better focusing performance, in terms of focal spot size and forming other complex-shaped patterns. The most straightforward method to enlarge the focusing array is to increase the number of elements. However, it will vastly increase the cost, the weight, and the feeding network complexity. One can enlarge interelement spacing to reduce the number of elements, although interelement spacing larger than half a wavelength usually leads to high sidelobe levels (SLLs) and grating lobes [9]–[13]. Thus, it is important to synthesize a large array with sparse configuration, low SLL, no grating lobes, and the capability of generating shaped beams.

To the best of the authors' knowledge, unlike the sophisticated methods for synthesizing sparse far-field patterns [14]–[17], there are only a few studies dealing with sparse arrays in the near-field region. Subsampled distribution is adopted [18] to enlarge element spacing, whereas the selection of spacing is based on empirical experience and it only deals with the generation of pseudo-Bessel beam. A subarray-based focused array antenna [19] is proposed to reduce the number of antenna elements, but it has a high SLL and its design is also based on empirical experiences. The genetic algorithm is adopted in [20] to synthesize a sparse array with controllable SLL. However, it is not effective and stochastic optimization is time-consuming and faces the problem of local convergence.

The multitask Bayesian compressive sensing (MT-BCS)-based methodology has been successfully generalized for both complex-value planar [21] and conformal arrays [22] radiating desired far-field patterns. Enlightened by these methods, an effective approach to deal with NFF problems is presented in this paper. The generalization of MT-BCS to the NFF case is challenging due to the following factors.

1) The BCS-based method needs a reference pattern to be matched. Unlike the sophisticated synthesis methods in the far-field region, there are only a few methods to synthesize a shaped pattern in the near-field region. Contour beam can be generated in [23], but it is ineffective to achieve a desired SLL. An effective approach would be required to employ the BCS-based method.
2) Unlike the finite solution space in the spherical coordinate system for the far-field synthesis problem, the solution space of NFF is an infinite plane defined by the Cartesian coordinate system parallel to the antenna aperture.

An appropriate reference pattern sampling strategy is required for the practicability and convergence of the algorithm. Moreover, sparse array synthesis usually leads to element clusters where elements are closely spaced, which makes the sparse layout impracticable. Element mutual coupling (MC) will result in the decrease of efficiency and the degradation of beam quality [24], which is usually even worse than the far-field case due to the complex problem at hand. A postprocessing of the final array excitation is necessary to put constraints on the minimum element spacing and compensate the MC effect.

Manuscript received March 7, 2018; revised June 29, 2018; accepted July 19, 2018. Date of publication July 26, 2018; date of current version October 4, 2018. This work was supported in part by the National Natural Science Foundation of China under Grant 61622105 and Grant 61631012 and in part by the Science Foundation for Distinguished Young Scholars of Sichuan Province under Grant 2015JQO005. *(Corresponding author: Yu Jian Cheng.)*

The authors are with the EHF Key Laboratory of Fundamental Science, School of Electronic Science and Engineering, University of Electronic Science and Technology of China, Chengdu 611731, China (e-mail: hzxaellen@gmail.com; chengyujian@uestc.edu.cn).

Color versions of one or more of the figures in this paper are available online at http://ieeexplore.ieee.org.

Digital Object Identifier 10.1109/TAP.2018.2860044

Referring to the challenges listed earlier, an effective approach synthesizing near-field patterns is proposed in this paper.

The remainder of this paper is organized as follows. In Section II, an approach synthesizing a reference near-field pattern is proposed. The near-field sparse array synthesis problem is then formulated based on MT-BCS and the synthesis procedure including the formulation of the solver to MT-BCS and array postprocessing is presented. Numerical results are presented to validate the effectiveness of the proposed method in Section III. Finally, the conclusions are drawn in Section IV.

II. Near-Field Sparse Array Synthesis Problem

A. Reference Pattern Synthesis

A reference pattern is required when synthesizing a sparse NFF array based on the BCS. Enlightened by [25], where the Taylor tapering and Woodward–Lawson method are combined to synthesize far-field patterns, an effective approach is proposed to generate NFF reference patterns of the linear co-polarization component with controllable SLLs.

Let us consider a planar focusing array with Q uniformly positioned elements and a focal distance z. The electric field radiated by the planar array at the observation point $E(r, r_f)$, in the near-field region, can be expressed as

$$E(r, r_f) = \sum_{q=1}^{Q} a_q E_q(r) = \sum_{q=1}^{Q} a_q F_q(r) \frac{e^{-j2\pi|r-r_q|/\lambda}}{|r-r_q|} \quad (1)$$

where r is the near-field observation position, r_f is the position of the focus point, and r_q is the position of the qth element. a_q denotes the complex excitation coefficient of the qth element. λ is the free-space wavelength. $F_q(r)$ is the required polarization component of the electric field radiated by the qth element at the observation position r, normalized with respect to the propagation factor $e^{-j2\pi R}/R$, with $R = |r - r_q|$.

The synthesis method has the following four steps.

First, find the excitation of a low SLL NFF array implementing NFF phasing and low SLL amplitude distribution such as Chebyshev or Taylor tapering, which can be found in detail in [26].

Second, the shaping pattern can be considered as a weighted superposition of several NFF patterns. Suppose that there are M patterns, whose weights are $(b_1, b_2, \ldots, b_M)$. By substituting the focusing point position r_f in (1) with $(r_{f1}, r_{f2}, \ldots, r_{fM})$, the shaping NFF pattern $E_{ref}(r)$ can be expressed as

$$E_{ref}(r) = \sum_{m=1}^{M} b_m E(r, r_{fm}). \quad (2)$$

Third, the value of $r_{f1}, r_{f2}, \ldots, r_{fM}$ needs to be determined. The shaping beam is sampled with uniform distance. Once, step 1 is finished, the half-power beamwidth $2B_{x0.5}$ and $2B_{y0.5}$ along each dimension of the NFF pattern can be extracted from the calculated pattern. It should be noted that the NFF patterns focusing on M different positions have different beamwidths, but they can be considered the same as the differences are usually small compared to the beamwidths. The number of sampling points can then be obtained by

$$\begin{cases} M_x \geq \dfrac{B_{Sx0.5}}{B_{x0.5}} + 1 \\ M_y \geq \dfrac{B_{Sy0.5}}{B_{y0.5}} + 1 \end{cases} \quad (3)$$

where $2B_{Sx0.5}$ and $2B_{Sy0.5}$ are the half-power beamwidths along the x- and y-directions of the shaping beam. The total number of sampling points is $M = M_x \times M_y$.

The fourth step is to determine the weights $(a_1, a_2, \ldots, a_M)$. Equation (2) can be discretized as expressed in the following matrix form:

$$E_{ref} = u\mathbf{AP} \quad (4)$$

where

$$\mathbf{P} = \begin{pmatrix} E_1(r_{o1}) & \cdots & E_Q(r_{o1}) \\ \vdots & \ddots & \vdots \\ E_1(r_{oK}) & \cdots & E_Q(r_{oK}) \end{pmatrix} \quad (5)$$

$$\mathbf{A} = \begin{pmatrix} a_1 e^{jk|r_{f1}-r_1|} & \cdots & a_Q e^{jk|r_{f1}-r_Q|} \\ \vdots & \ddots & \vdots \\ a_1 e^{jk|r_{fM}-r_1|} & \cdots & a_Q e^{jk|r_{fM}-r_Q|} \end{pmatrix} \quad (6)$$

$$u = (b_1, b_2, \ldots, b_M). \quad (7)$$

There are K observation points in the target-shaping plane in the near-field region with their position in the near-field region being r_{ok}, $k = 1, \ldots, K$. u can then be determined through solving the following optimization problem:

$$u = \arg(\min_u \|E_{ref\_ml} - M_{ml}\|_2) \quad \text{s.t. } q \in \Re^+ E_{ref\_sl} \leq M_{sl} \quad (8)$$

where E_{ref_ml} is the mainlobe part while E_{ref_sl} is the sidelobe part of E_{ref}, and M_{ml} is the mainlobe pattern or mask while M_{sl} is the desired sidelope mask of the target near-field pattern. The final excitations of the array can be effectively solved by CVX [27].

B. Near-Field Sparse Array Synthesis Definition

Once we obtain a near-field reference pattern, we can define the sparse array synthesis problem as follows. Let us consider a planar array with S elements whose sth element is located at r_s with excitation w_s, $s = 1, \ldots, S$, such that S is the minimum and the near-field pattern matches a desired pattern $E_{ref}(r)$, in a set of K observation positions in the near-field region, r_{ok}, $k = 1, \ldots, K$, within a given matching threshold ε. Furthermore, we assume that the S elements belong to a user-defined dense grid with N candidate elements, $N \ll S$, whose nth element is located at r_n with the normalized element pattern $F_n(r)$. Here, we assume that the antenna element is a y-oriented short dipole, and its radiation pattern can be found in [28]. It is worth mentioning that only the far-field component of the short dipole is taken into consideration, as it is assumed that the near-field observation point is in the far-field region of each array element when $|r - r_n| > \lambda$. For a typical NFF antenna, its focal distance lies in the Fresnel zone [26], [28], [29], which usually satisfies this condition.

The similar assumption can also be found in [28] and [29]. Under the assumptions discussed earlier, the near-field sparse array synthesis problem can be formulated as

$$w = \arg(\min_{w} \|w\|_0) \quad \text{s.t. } E_{ref} - \mathbf{\Phi} w = e \tag{9}$$

where $w = (w_1, \ldots, w_N)^{\mathrm{T}}$ is the excitation vector of the dense array, and $E_{ref} = [E_{ref}(r_{o1}), \ldots, E_{ref}(r_{oK})]^{\mathrm{T}}$ is a sampled vector of the reference near-field pattern at different K observation positions. e is the zero-mean Gaussian error vector whose variance is σ^2, and it is proportional to the pattern matching tolerance ε. Equation (10), as shown at the bottom of the page, is the kernel matrix for the NFF problem.

The problem stated by (9) is a nondeterministic polynomial-time hard problem, which cannot be easily solved by deterministic approaches. The stochastic optimizer may be a candidate to solve the problem, but it faces the problem of local convergence and it is not effective due to the complex high-dimensional problem at hand. MT-BCS has proven to be an effective solver for complex-value sparse problems in the studies dealing with far-field sparse array syntheses. To solve (9) by MT-BCS, the complex-value near-field sparse array synthesis problem is reformulated as a probabilistic problem as follows [21]:

$$w_G = \arg \ (\max_{w_G}[p(w_G|E_G)]) \quad G = R, I \tag{11}$$

where the real part and the imaginary part of the excitation w are considered as two real vectors. Equation (9) is further rewritten in the following matrix form:

$$\begin{cases} E_R = \begin{bmatrix} R(\mathbf{\Phi}) \\ I(\mathbf{\Phi}) \end{bmatrix} w_R + e_R \\ E_I = \begin{bmatrix} -I(\mathbf{\Phi}) \\ R(\mathbf{\Phi}) \end{bmatrix} w_I + e_I \end{cases} \tag{12}$$

where $w = w_R + j w_I$. $E_R + E_I[R(E_{ref}), I(E_{ref})]^{\mathrm{T}}$, $e_R + e_I = [R(e), I(e)]^{\mathrm{T}}$, and $R(\bullet)$ and $I(\bullet)$ indicates the real and the imaginary parts, respectively.

C. Excitation Determination Through MT-BCS

It has been deeply discussed in [21], [22], and [30] that both single-task (ST) BCS and MT-BCS can be applied to solve (11). MT-BCS usually outperform ST-BCS when dealing with complex-value problems. Specifically, the near-field sparse focusing array synthesis problem at hand is a complex-value problem. The probabilistic MT-BCS [31] is then customized for the near-field case

$$p(w_G|E_G) = \int p(w_G|E_G, \alpha) p(\alpha|E_G) d\alpha \quad G = R, I \tag{13}$$

where α is the hyperparameter vector that statistically accounts for the relationships between the real and imaginary parts of the array excitation. The value of w can be determined by

$$\begin{cases} w_R = [\mathrm{diag}(\underline{\alpha}) + [R(\mathbf{\Phi}), I(\mathbf{\Phi})][R(\mathbf{\Phi}), I(\mathbf{\Phi})]^{\mathrm{T}}] \\ \qquad \times [R(\mathbf{\Phi}), I(\mathbf{\Phi})] E_R \\ w_I = [\mathrm{diag}(\underline{\alpha}) + [-I(\mathbf{\Phi}), R(\mathbf{\Phi})][-I(\mathbf{\Phi}), R(\mathbf{\Phi})]^{\mathrm{T}}] \\ \qquad \times [-I(\mathbf{\Phi}), R(\mathbf{\Phi})] \underline{E_I} \end{cases} \tag{14}$$

where $\underline{\alpha}$ is the hyperparameter determined by maximizing the logarithm of the likelihood

$$L(\alpha) = -\frac{1}{2} \log \left\{ |\mathbf{B}_R| |\mathbf{B}_I| \left[\left(\underline{E}_R^{\mathrm{T}} \mathbf{B}_R^{-1} \underline{E}_R + 2\beta_2 \right) \times \left(E_I^{\mathrm{T}} \mathbf{B}_I^{-1} \underline{E}_I + 2\beta_2 \right) \right]^{N+2\beta_1} \right\} \tag{15}$$

where $\mathbf{B}_R = \mathbf{I} + [R(\mathbf{\Phi}), I(\mathbf{\Phi})]^{\mathrm{T}} \mathrm{diag}(\alpha)^{-1} [R(\mathbf{\Phi}), I(\mathbf{\Phi})]$ and $\mathbf{B}_I = \mathbf{I} + [-I(\mathbf{\Phi}), R(\mathbf{\Phi})]^{\mathrm{T}} \mathrm{diag}(\alpha)^{-1} [R(\mathbf{\Phi}), I(\mathbf{\Phi})]$. β_1 and β_2 are the user-defined control parameters. Once the reformulation occurs, a type-II maximum likelihood procedure can be performed to estimate the hyperparameters, which can be implemented via the fast relevance vector machine algorithms online [32].

D. Elements and Pattern Sampling Strategy

It is important to have an appropriate sampling strategy in order to guarantee the convergence of the proposed method. The solution space of the far-field synthesis problem is finite, defined by the spherical coordinate system, which is usually the upper hemisphere of the antenna aperture, where $\theta < 90^\circ$ and $\varphi \in [0^\circ, 360^\circ]$. However, the synthesis domain for NFF is an infinite plane parallel to the antenna aperture, defined by the Cartesian coordinate system. Hence, the sampling strategies in [21] and [22] for the far-field synthesis problem are no longer applicable to the NFF problem, as such strategies would result in an infinite number of sampling points.

According to the near-field sparse array synthesis problem at hand, the criteria for creating a candidate element grid and the strategy to sample the reference near-field pattern, i.e., the observation positions, need to be clarified at the beginning. As it is illustrated in Fig. 1, we adopt a planar uniform grid for candidate elements. The reference pattern, which lies on an infinite plane parallel to the antenna aperture, is sampled by the following strategy. The equation physically means that the solution space, with a truncation angle T, is equally divided into k angles and projected to the focal plane, with

$$\mathbf{\Phi} = \begin{pmatrix} F_1(r) \dfrac{\exp(-j2\pi |r_{o1} - r_1|/\lambda)}{|r_{o1} - r_1|} & \cdots & F_N(r) \dfrac{\exp(-j2\pi |r_{o1} - r_N|/\lambda)}{|r_{o1} - r_N|} \\ \vdots & \ddots & \vdots \\ F_1(r) \dfrac{\exp(-j2\pi |r_{oK} - r_1|/\lambda)}{|r_{oK} - r_1|} & \cdots & F_N(r) \dfrac{\exp(-j2\pi |r_{oK} - r_N|/\lambda)}{|r_{oK} - r_N|} \end{pmatrix} \tag{10}$$

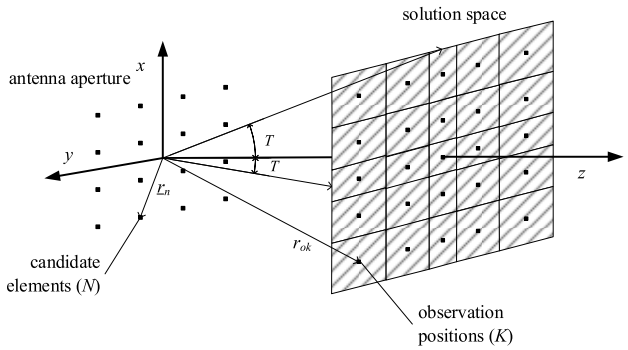

Fig. 1. Illustration of a near-field focus problem, where the reference pattern in the synthesis plane is sampled by (16) and it is radiated by N candidate elements.

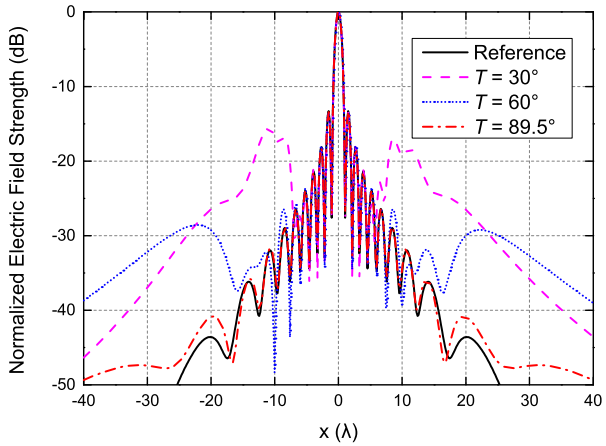

Fig. 2. Sparse focused pattern with different T.

the projected points being the observation points

$$\begin{cases} x_k = z \times \tan\left(\dfrac{2T(k \bmod K_x)}{K_x - 1} - T\right) \\ y_k = z \times \tan\left(\dfrac{2T\left[\frac{k}{K_x}\right]}{K_y - 1} - T\right) \\ z_k = z \end{cases} \tag{16}$$

where z is the distance between the focal plane and the array aperture, $[\bullet]$ denotes the integer value of $\bullet$, and T is the truncation factor in degrees, $K_x \times K_y = K$, and $k = 1, \ldots, K$.

As it is mentioned earlier, the solution space is infinite due to the NFF problem at hand. An appropriate truncation of the synthesis plane is needed to make the pattern constrained in the solution space and at the same time make the proposed method practicable. The truncation can be achieved by properly selecting the truncation angle T.

The following three numerical examples are presented in Fig. 2 to demonstrate the selection of T. For simplicity, a 10λ linear NFF array with focal distance $z = 10\lambda$ is considered. T is first set to be 30° and there is a noticeable unconstrained space, $|x| > z \times \tan(30°) = 5.77\lambda$, where greater sidelobes appear. This can be avoided by enlarging T. T is then set to be 60° and the peak sidelobe level (PSL) is -28.57 dB outside the solution space in $|x| > 17.32\lambda$. A larger T is preferred to ensure that the pattern is well constrained in the solution space. It is worth mentioning that T cannot reach 90°, as this would cause x_k and y_k to become infinite, preventing numerical computations from being performed. Therefore, $T = 89.5°$ is adopted in the rest of our design.

E. Minimum Spacing Constraint

Sparse array synthesis including MT-BCS [14], [16], [21], [22] can lead to element clusters where elements are closely spaced, which makes the array impractical. It is worth mentioning that the clusters are caused by the discretization of the candidate elements grid, and it is impracticable to simply have a denser grid as the computational cost will vastly increase at the same time. As the elements are extremely close, they can be considered as a single element. The postprocessing method, e.g., element merging, is used in [22] and [33] as a constraint for the minimum element spacing, where closely spaced elements are replaced by a single element. However, the introduction of the postprocessing method will inevitably deteriorate the pattern matching accuracy.

In order to enforce an acceptable minimum element spacing constraint, with u being the minimum spacing, and at the same time mitigate the pattern deterioration, element merging is performed for element locations and then a convex optimization is utilized to reestimate the optimal excitations for the merged scenario. The postprocessing procedure is based on the following four steps.

1) Set $p = 1$, $S_i = S$, and count $= 0$. Here, count denotes the number of times that two close elements are merged within each iteration.
2) Find the closest element $\underline{r}_c$ to $\underline{r}_p$, with its excitation w_c. If $|\underline{r}_c - \underline{r}_p| < u$, update $\underline{r}_p = (|w_c|\underline{r}_c + |w_p|\underline{r}_p)/(|w_c| + |w_p|)$, count $=$ count $+ 1$ and then set $\underline{r}_c = \infty$ from the aperture and $p = p + 1$, repeat step 2. If $|\underline{r}_c - \underline{r}_p| > u$, $p = p + 1$, repeat step 2.
3) If $p = S_i$ and count $= 0$, it means that all elements are checked and no merging occurs within one iteration, then go to step 4. Else if $p = S_i$ and count > 0, delete all the elements which are set to be ∞, then update S_i with the number of the merged sparse layout, set $p = 1$, count $= 0$, and go to step 2 to check the merged layout again.
4) Consider the following convex optimization, the final excitation can be estimated by solving (17) to match the target reference near-field pattern, which can be effectively solved by CVX [27]

$$w_f = \arg(\min_{w_f} \|\mathbf{\Phi}_f w_f - E_{ref}\|_2) \tag{17}$$

where $\mathbf{\Phi}_f$ is the kernel matrix of the merged array, and w_f denotes the final array excitation.

F. Mutual Coupling Compensation

Antenna MC will result in the reduction of efficiency and the degradation of beam quality [23], [24], [26]. For a $5\lambda \times 5\lambda$ focused array, a comparison between the synthesized focusing pattern (without MC) and the pattern calculated by the method-of-moment-based commercial software FEKO (with MC) is illustrated in Fig. 3. Noticeable degradation can be observed, where PSL increases to -16.8 from -20 dB.

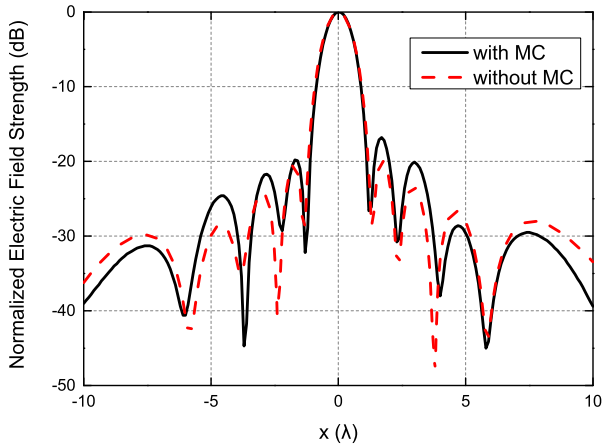

Fig. 3. MC effect in NFF problem.

TABLE I
MC DEPENDENT ON FOCAL DISTANCE

Focal Distance (λ)	PSL (dB)	PSL_MC (dB)
7.5	–19.09	–17.10
10	–20.28	–16.80
12.5	–21.41	–18.80
15	–22.34	–17.24
17.5	–22.81	–19.00
20	–23.40	–19.40

Moreover, a numerical analysis is performed for different sparse arrays, which have the same overall aperture size $10\lambda \times 10\lambda$ but with different focal distance. The comparison in Table I shows that there is no apparent dependence on the focal distance for sparse NFF arrays. This is due to the pattern degradation being related to both the focal distance and the actual sparse layout. However, the results prove that MC cannot be neglected for NFF sparse arrays.

The excitation weights obtained by Section II-E are multiplied with the FEKO-computed impedance matrix $\boldsymbol{Z}$ to take MC into account. The final array excitation w_{f_com} with MC compensated can be expressed by

$$w_{f\_com} = \mathbf{Z} w_f. \tag{18}$$

III. NUMERICAL RESULTS

In this section, several numerical examples are presented to validate the effectiveness of the proposed method.

The normalized mean square error ξ is calculated by the following expression to quantitatively evaluate the method's performance:

$$\xi = \frac{\|\boldsymbol{\Phi}_f w_f - E_{ref}\|_2^2}{\|E_{ref}\|_2^2}. \tag{19}$$

Moreover, the sparsity of the synthesized array is defined by $\gamma = S_f/S_{uni}$, where S_{uni} is the number of elements with uniform spacing $\lambda/2$ generating the reference near-field pattern. $\Delta L_{\min}$ denotes the minimum element spacing and ΔL_{ave} is the average spacing.

To this end, it should be noted that a rigid theoretical analysis of the matching error ξ and sparsity γ against a certain control parameter still remains to be an open challenge due to the unavailability of analytical expressions between them. An acceptable tradeoff range of these parameters for the near-field case is found as below through careful calibrations and following the guidelines in [21] and [22]: $N \in (225S_{uni}, 400S_{uni})$, $K \in (4S_{uni}, 9S_{uni})$, $\beta_1 \in (10^3, 10^4)$, and $\beta_2 \in (1, 10)$.

TABLE II
COMPARATIVE ANALYSIS FOR DIFFERENT INTERELEMENT SPACING

u (λ)	ξ (10^{-3})	γ	$\Delta L_{\min}/\lambda$	$\Delta L_{\text{ave}}/\lambda$
0.10	3.0	0.56	0.11	0.77
0.20	3.4	0.51	0.21	0.86
0.30	3.7	0.49	0.38	0.88
0.40	4.9	0.47	0.42	0.89
0.50	7.0	0.43	0.52	0.92
0.60	29.5	0.37	0.61	0.95
0.70	159.9	0.29	0.71	1.07

TABLE III
COMPARATIVE ANALYSIS FOR A DIFFERENT LATTICE SPACING

h (λ)	ξ (10^{-3})	γ	$\Delta L_{\min}/\lambda$	$\Delta L_{\text{ave}}/\lambda$
0.0125 with merging	7.0	0.43	0.52	0.92
0.42	9.2	0.64	0.42	0.68
0.50	8.0	0.52	0.50	0.76
0.63	6.2	0.57	0.63	0.71
0.71	13.6	0.53	0.71	0.80

A. Low SLL Focused Pattern

As a preliminary example, we consider a low SLL near-field focused beam pattern. The reference pattern is obtained by a focused $5\lambda \times 5\lambda$ planar array with the interelement spacing of $0.5\lambda (S_{uni} = 121)$ focusing at a focal distance 5λ. It uses a farfield -25 dB Taylor amplitude tapering and the actual PSL of the near-field pattern is -20 dB. The final sparse layout is based on both the candidate element spacing and minimum interelement spacing u. Let us consider the case that a small candidate element spacing, 0.0125λ, is selected. Then, an appropriate selection of u for the element merger is needed. Specifically, a parametrical sweeping of u is performed to match the reference focused pattern. The comparative results are listed in Table II. As it can be expected, more elements are needed and the pattern matching accuracies are better with smaller interelement spacing. Here, we adopt 0.5λ in the rest of our designs, as it is a common setting that makes the array practicable. Moreover, the matching accuracy is acceptable for 0.5λ.

The aforementioned element merger is proposed to put a constraint on the minimum interelement spacing ensuring that the array is practicable. One can also enlarge the candidate element spacing, lattice spacing h, to ensure the array practicability. A comparative analysis between the proposed approach and the other option of setting h for avoiding unfeasible element positions (without the element merger and still applying later on the CVX reestimating the excitation) is performed. The numerical result in Table III, where $u = 0.5\lambda$, is set as the benchmark for the quantitative evaluation. The comparative results are listed in Table III. It can be noticed that the proposed method, where smaller h is selected and an

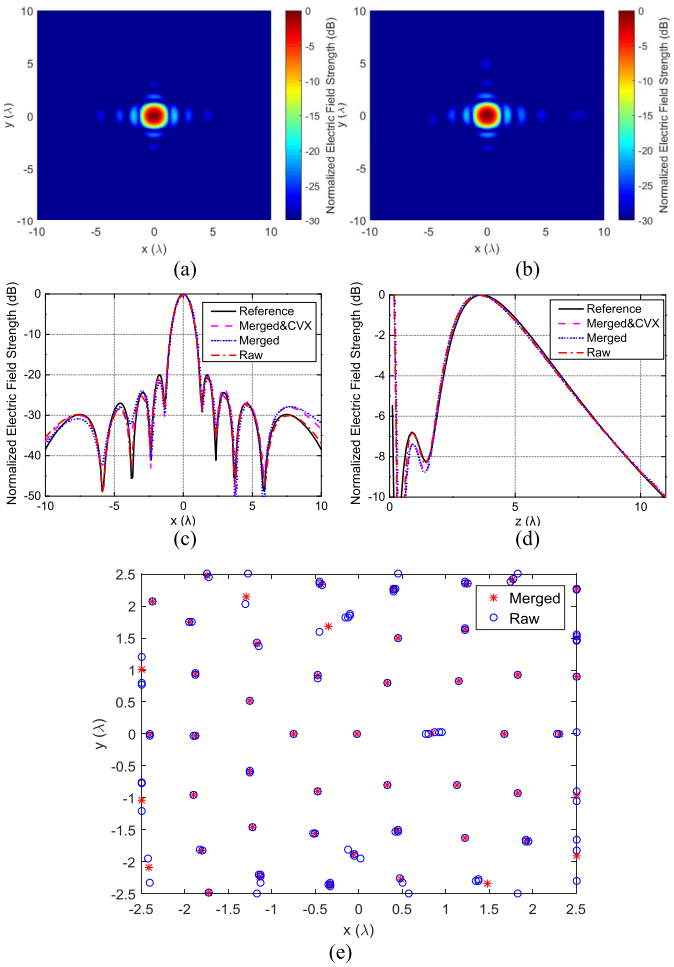

Fig. 4. Focused pattern. (a) Synthesized pattern. (b) Reference pattern. (c) Pattern comparison at $y = 0$ cut. (d) Focusing performance along the z-direction. (e) Sparse layout of the raw data (without merging) and the merged array.

TABLE IV
PERFORMANCE COMPARISON FOR A FOCUSED PATTERN

	$\xi\,(10^{-3})$	PSL (dB)	γ	$\Delta L_{\min}/\lambda$	$\Delta L_{ave}/\lambda$
Raw	4.1	–20.32	0.95	2.5×10^{-2}	0.60
Merged	9.2	–20.30	0.43	0.52	0.92
Merged & CVX	7.0	–20.01	0.43	0.52	0.92

extra merger is adopted, is more likely to find the sparsest layout with acceptable matching accuracy.

$h = 0.0125\lambda$ and $u = 0.5\lambda$ are chosen for the final setting. The reference pattern and synthesized pattern of the focal plane are shown in Fig. 4(a) and (b). It can be noted that the proposed method has well matched the reference pattern. Moreover, to demonstrate the effectiveness of the element merger and the convex optimization, Fig. 4(c)–(e) and Table IV are presented in this paper, where raw stands for the sparse layout directly obtained from MT-BCS without merging. Clustered elements can be seen in Fig. 4(e), which will reduce the sparsity of the layout, as it can be found that 115 ($\gamma = 00.95$) elements are needed, and at the same time make the sparse layout impracticable, where $\Delta L_{\min}/\lambda = 2.5\times 10^{-2}$. An extra merger described in Section II-E is employed

TABLE V
SPARSE LAYOUT DEPENDENCE ON FOCAL DISTANCE

Focal Distance (λ)	$\xi\,(10^{-2})$	γ	$\Delta L_{\min}/\lambda$	$\Delta L_{ave}/\lambda$
7.5	1.24	0.44	0.50	0.90
10	1.21	0.42	0.50	0.95
12.5	1.05	0.41	0.50	0.96
15	1.02	0.39	0.50	0.95
17.5	0.84	0.37	0.51	0.97
20	1.04	0.35	0.50	1.01

and a sparse layout with a significantly reduced number of elements ($S_f = 52, \gamma = 0.43$) is obtained in Fig. 4(e), where $\Delta L_{\min}/\lambda = 0.52$ and $\Delta L_{ave}/\lambda = 0.92$. Noticeable pattern degradation occurs after merging the element, where the matching error ξ drops from 4.1×10^{-3} to 9.2×10^{-3}. However, with the convex optimization reestimating the excitation to match the reference pattern, the degradation is mitigated and ξ decreases to 7.0×10^{-3}. Furthermore, the focusing performance along the z-direction is illustrated in Fig. 4(d), where the synthesized result faithfully matches the reference pattern. The data listed in Table IV validate the effectiveness of the postprocessing of the final array excitation, which helps maintain good performance and ensures the practicability of the sparse layout.

Different from the far-field synthesis, the sparse layout of an NFF array also depends on the focal distance. An analysis of such dependence is also performed. For the fair comparison, the aperture size of the array is fixed ($10\lambda \times 10\lambda$) with the desired ξ of around 0.01. The reference patterns are obtained by the excitation with the same amplitude. The focal distance of the reference pattern is altered by modifying the phase of excitation. Different layouts are obtained for different focal distance and the comparison is shown in Table V. It can be noted that fewer elements are needed for greater focal distance. This is due to for a fixed size NFF array, the 3 dB beamwidth being smaller at a greater focal distance [34] and less degrees of freedom being required to generate a wider focused beam.

B. Flat-Top Pattern

As a second example, we consider a near-field flat-top pattern. The reference pattern is obtained by the proposed method in Section II-A. The array aperture is a $10\lambda \times 10\lambda$ planar array with the interelement spacing of 0.5λ ($S_{uni} = 441$) and a target-shaping plane 10λ away from the aperture. The reference flat-top pattern has its half-power area in $5.6\lambda \times 5.6\lambda$ of the focusing plane with a PSL $= -26.13$ dB. The synthesized pattern without the final convex optimization has a PSL $= -20.44$ dB, which is much higher than the reference pattern due to degradation caused by the extra merger. However, the PSL decreases to –23.41 dB and more importantly, in terms of matching error, it drops from 10.2×10^{-3} to 5.3×10^{-3}, showing that the convex optimization does help to improve the matching performance. The synthesized pattern in Fig. 5(b), which has a significant reduction of elements ($S_f = 171, \gamma = 0.39$) compared to the raw data ($S_f = 397, \gamma = 0.90$), matches well with the reference

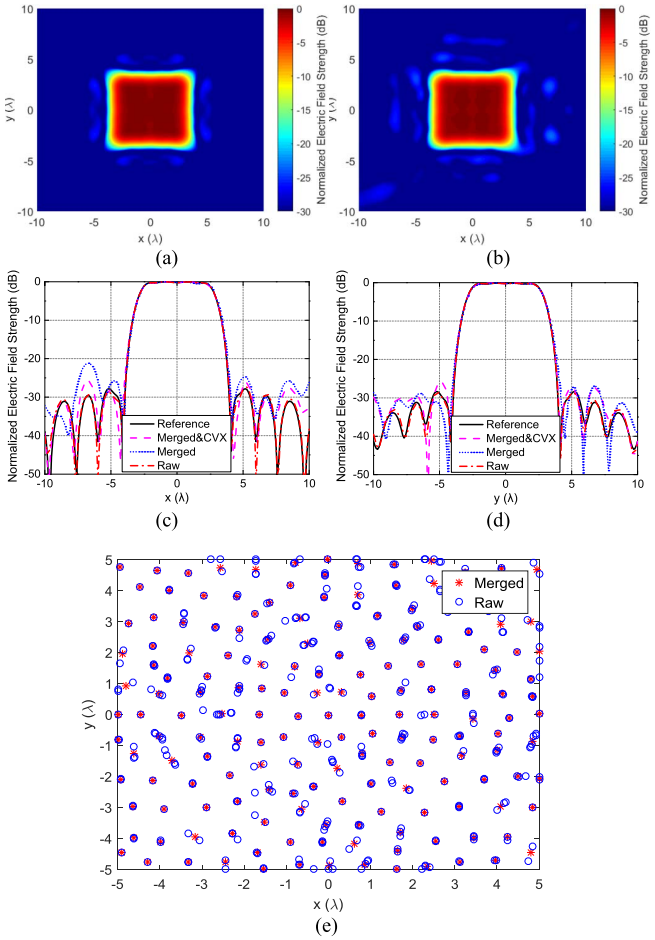

Fig. 5. Flat-top pattern. (a) Synthesized pattern. (b) Reference pattern. Pattern comparison at (c) $y = 0$ cut and (d) $x = 0$ cut. (e) Sparse layout of the raw data (without merging) and the merged array.

TABLE VI

PERFORMANCE COMPARISON FOR A FLAT-TOP PATTERN

	$\xi\,(10^{-3})$	PSL (dB)	γ	$\Delta L_{\min}/\lambda$	$\Delta L_{\text{ave}}/\lambda$
Raw	0.26	–26.18	0.90	2.5×10^{-2}	0.65
Merged	10.2	–20.44	0.39	0.50	0.96
Merged & CVX	5.3	–23.41	0.39	0.50	0.96

pattern, though an acceptable deviation can be noted. The performance comparison for a flat-top pattern based on different methods is listed in Table VI.

C. Linear Amplitude Taper Pattern

To further demonstrate the effectiveness and flexibility of the proposed method, an area of $5.2\lambda \times 5.2\lambda$ with linear amplitude taper is considered. The reference pattern is obtained by a $10\lambda \times 10\lambda$ planar array with the interelement spacing of $0.5\lambda (S_{uni} = 441)$ and the target linear amplitude tapered plane is 10λ away from the aperture. A faithful matching to the reference pattern can be observed in Fig. 6 and Table VII with an acceptable deviation. The numerical results of Sections III-B and III-C prove the effectiveness of the proposed method for synthesizing complex-shaped beams in the NF region.

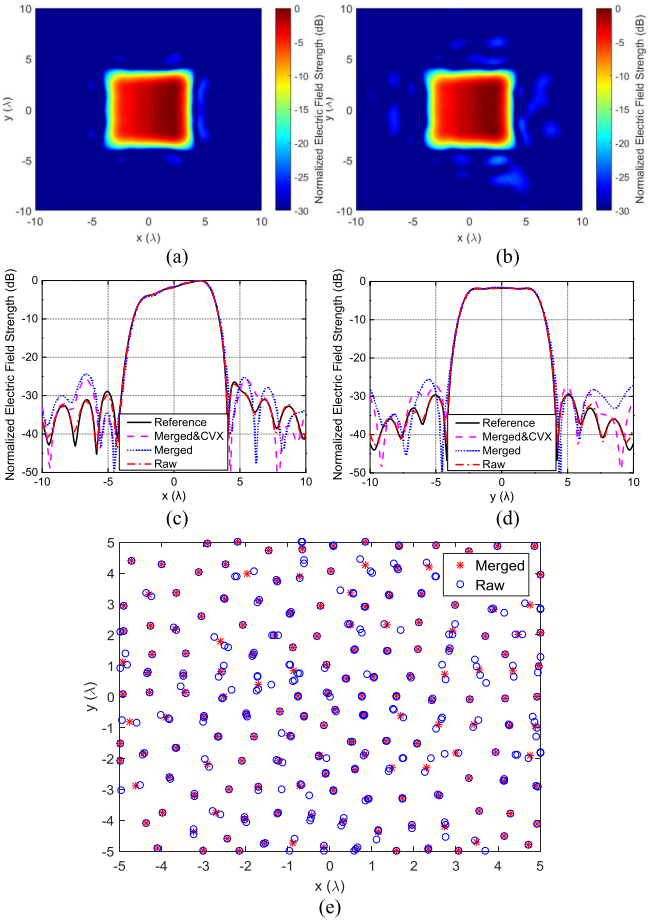

Fig. 6. Linear amplitude tapered pattern. (a) Synthesized pattern. (b) Reference pattern. Pattern comparison at (c) $y = 0$ cut and (d) $x = 0$ cut. (e) Sparse layout of the raw data (without merging) and the merged array.

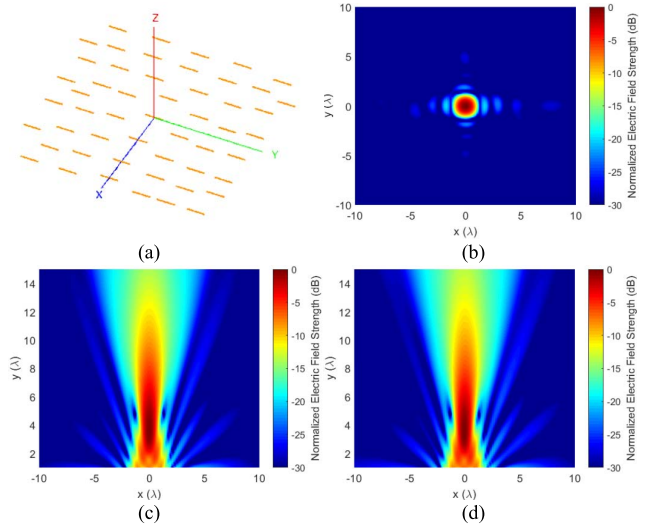

Fig. 7. Synthesized and FEKO-simulated near-field focused pattern. (a) Sparse dipole layout. (b) FEKO-simulated pattern at the focal plane. (c) Synthesized pattern at the *xoz* plane. (d) FEKO-simulated pattern at the *xoz* plane.

D. Sparse Array With Mutual Coupling

A realistic array of the presented numerical example, the focused pattern in Section III-A, is simulated by the commercial software FEKO. Its actual array excitation is

TABLE VII
PERFORMANCE COMPARISON FOR A LINEAR AMPLITUDE TAPERED PATTERN

	ξ (10^{-3})	PSL (dB)	γ	$\Delta L_{\min}/\lambda$	$\Delta L_{\text{ave}}/\lambda$
Raw	0.42	–24.50	0.76	2.5×10^{-2}	0.69
Merged	10.9	–22.71	0.38	0.50	0.98
Merged & CVX	6.8	–22.75	0.38	0.50	0.98

obtained by multiplying the synthesized excitations with an impedance matrix that accounts for the MC calculated by FEKO. As depicted in Fig. 7, FEKO-simulated results agree well with the patterns calculated by the proposed method, which shows that this method is effective for practical applications.

IV. CONCLUSION

An effective method based on MT-BCS and convex optimization is proposed in this paper for near-field sparse array synthesis problem. Three near-field examples are presented to validate the proposed method. The significant reduction of the number of elements is achieved with more than 50% of the elements saved compared to the $\lambda/2$ uniformly spaced layout.

REFERENCES

[1] H.-Y. Zhang, F.-S. Zhang, F. Zhang, F.-K. Sun, and G.-J. Xie, "High-power array antenna based on phase-adjustable array element for wireless power transmission," *IEEE Antennas Wireless Propag. Lett.*, vol. 16, pp. 2249–2253, 2017.

[2] Y. J. Cheng and F. Xue, "Ka-band near-field-focused array antenna with variable focal point," *IEEE Trans. Antennas Propag.*, vol. 64, no. 5, pp. 1725–1732, May 2016.

[3] Y. C. Zhong and Y. J. Cheng, "Wideband Quasi-nondiffraction beam with accurately controllable propagating angle and depth-of-field," *IEEE Trans. Antennas Propag.*, vol. 65, no. 10, pp. 5035–5042, Oct. 2017.

[4] Y. C. Zhong and Y. J. Cheng, "Ka-band wideband large depth-of-field beam generation through a phase shifting surface antenna," *IEEE Trans. Antennas Propag.*, vol. 64, no. 12, pp. 5038–5045, Dec. 2016.

[5] A. Buffi, A. A. Serra, P. Nepa, and G. Manara, "A focused planar microstrip array for 2.4 GHz RFID readers," *IEEE Trans. Antennas Propag.*, vol. 58, no. 5, pp. 1536–1544, May 2010.

[6] J. T. Loane and S.-W. Lee, "Gain optimization of a near-field focusing array for hyperthermia applications," *IEEE Trans. Microw. Theory Techn.*, vol. 37, no. 10, pp. 1629–1635, Oct. 1989.

[7] A. J. Martinez-Ros, J. L. Gómez-Tornero, and G. Goussetis, "Holographic pattern synthesis with modulated substrate integrated waveguide line-source leaky-wave antennas," *IEEE Trans. Antennas Propag.*, vol. 61, no. 7, pp. 3466–3474, Jul. 2013.

[8] M. Ettorre *et al.*, "On the near-field shaping and focusing capability of a radial line slot array," *IEEE Trans. Antennas Propag.*, vol. 62, no. 4, pp. 1991–1999, Apr. 2014.

[9] D. L. Rudolph and W. C. Barott, "Reduction of near-field grating lobes in sparse linear phased arrays," in *Proc. IEEE Antennas Propag. Soc. Int. Symp. (APSURSI)*, Memphis, TN, USA, Jul. 2014, pp. 1155–1156.

[10] Y. J. Cheng, J. Wang, and X. L. Liu, "94 GHz substrate integrated waveguide dual-circular-polarization shared-aperture parallel-plate long-slot array antenna with low sidelobe level," *IEEE Trans. Antennas Propag.*, vol. 65, no. 11, pp. 5855–5861, Nov. 2017.

[11] J. Wu, Y. J. Cheng, and Y. Fan, "A wideband high-gain high-efficiency hybrid integrated plate array antenna for V-band inter-satellite links," *IEEE Trans. Antennas Propag.*, vol. 63, no. 4, pp. 1225–1233, Apr. 2015.

[12] Y. J. Cheng, W. Hong, and K. Wu, "94 GHz substrate integrated monopulse antenna array," *IEEE Trans. Antennas Propag.*, vol. 60, no. 1, pp. 121–128, Jan. 2012.

[13] H. B. Wang and Y. J. Cheng, "Frequency selective surface with miniaturized elements based on quarter-mode substrate integrated waveguide cavity with two poles," *IEEE Trans. Antennas Propag.*, vol. 64, no. 3, pp. 914–922, Mar. 2016.

[14] Y. Liu, Q. H. Liu, and Z. Nie, "Reducing the number of elements in the synthesis of shaped-beam patterns by the forward-backward matrix pencil method," *IEEE Trans. Antennas Propag.*, vol. 58, no. 2, pp. 604–608, Feb. 2010.

[15] G. Oliveri, M. Carlin, and A. Massa, "Complex-weight sparse linear array synthesis by Bayesian compressive sampling," *IEEE Trans. Antennas Propag.*, vol. 60, no. 5, pp. 2309–2326, May 2012.

[16] G. Prisco and M. D'Urso, "Maximally sparse arrays via sequential convex optimizations," *IEEE Antennas Wireless Propag. Lett.*, vol. 11, pp. 192–195, 2012.

[17] D. Pinchera, M. D. Migliore, F. Schettino, M. Lucido, and G. Panariello, "An effective compressed-sensing inspired deterministic algorithm for sparse array synthesis," *IEEE Trans. Antennas Propag.*, vol. 66, no. 1, pp. 149–159, Jan. 2018.

[18] P. Lemaitre-Auger, S. Abielmona, and C. Caloz, "Generation of Bessel beams by two-dimensional antenna arrays using sub-sampled distributions," *IEEE Trans. Antennas Propag.*, vol. 61, no. 4, pp. 1838–1849, Apr. 2013.

[19] P.-F. Li, S.-W. Qu, S. Yang, and Z.-P. Nie, "Focused array antenna based on subarrays," *IEEE Antennas Wireless Propag. Lett.*, vol. 16, pp. 888–891, Sep. 2016.

[20] G. Sun and Q. Zhu, "The design of a focused sparse microstrip antenna array," in *Proc. IEEE Int. Symp. Antennas Propag. (APSURSI)*, Fajardo, PR, USA, Jun./Jul. 2016, pp. 515–516.

[21] F. Viani, G. Oliveri, and A. Massa, "Compressive sensing pattern matching techniques for synthesizing planar sparse arrays," *IEEE Trans. Antennas Propag.*, vol. 61, no. 9, pp. 4577–4587, Sep. 2013.

[22] G. Oliveri, E. T. Bekele, F. Robol, and A. Massa, "Sparsening conformal arrays through a versatile BCS-based method," *IEEE Trans. Antennas Propag.*, vol. 62, no. 4, pp. 1681–1689, Apr. 2014.

[23] H.-T. Chou, N.-N. Wang, H.-H. Chou, and J.-H. Qiu, "An effective synthesis of planar array antennas for producing near-field contoured patterns," *IEEE Trans. Antennas Propag.*, vol. 59, no. 9, pp. 3224–3233, Sep. 2011.

[24] H.-S. Loi, H. T. Hui, and M. Persson, "Preliminary investigations of mutual coupling effect on near-field beam focusing," in *Proc. APMC*, Yokohama, Japan, Dec. 2010, pp. 1705–1708.

[25] J.-Y. Li, Y.-X. Qi, and S.-G. Zhou, "Shaped beam synthesis based on superposition principle and Taylor method," *IEEE Trans. Antennas Propag.*, vol. 65, no. 11, pp. 6157–6160, Nov. 2017.

[26] S. Karimkashi and A. A. Kishk, "Focused microstrip array antenna using a Dolph-Chebyshev near-field design," *IEEE Trans. Antennas Propag.*, vol. 57, no. 12, pp. 3813–3820, Dec. 2009.

[27] M. Grant and S. Boyd, *CVX: Matlab Software for Disciplined Convex Programming*. Accessed: Sep. 15, 2017. [Online]. Available: http://cvxr.com/cvx

[28] A. Buffi, P. Nepa, and G. Manara, "Design criteria for near-field-focused planar arrays," *IEEE Antennas Propag. Mag.*, vol. 54, no. 1, pp. 40–50, Feb. 2012.

[29] P. Nepa and A. Buffi, "Near-field-focused microwave antennas: Near-field shaping and implementation," *IEEE Antennas Propag. Mag.*, vol. 59, no. 3, pp. 42–53, Jun. 2017.

[30] G. Oliver and A. Massa, "Bayesian compressive sampling for pattern synthesis with maximally sparse non-uniform linear arrays," *IEEE Trans. Antennas Propag.*, vol. 59, no. 2, pp. 467–482, Feb. 2011.

[31] S. Ji, D. Dunson, and L. Carin, "Multitask compressive sensing," *IEEE Trans. Signal Process.*, vol. 57, no. 1, pp. 92–106, Jan. 2009.

[32] S. Ji, Y. Xue, and L. Carin, *Bayesian Compressive Sensing Code*. Accessed: Aug. 20, 2017. [Online]. Available: http://people.ee.duke.edu/~lcarin/BCS.html

[33] M. B. Hawes and W. Liu, "Compressive sensing-based approach to the design of linear robust sparse antenna arrays with physical size constraint," *IET Microw., Antennas Propag.*, vol. 8, no. 10, pp. 736–746, Jul. 2014.

[34] J. Sherman, "Properties of focused apertures in the Fresnel region," *IRE Trans. Antennas Propag.*, vol. 10, no. 4, pp. 399–408, Jul. 1962.

Zi Xuan Huang (S'16) was born in Dongguan, Guangdong, China, in 1994. He received the B.S. degree from the University of Electronic Science and Technology of China, Chengdu, China, in 2016, where he is currently pursuing the M.S. degree with the Department of Electronic Science and Engineering.

His current research interests include signal processing, optimization techniques, and conformal phased array antennas.

Yu Jian Cheng (SM'14) was born in Chengdu, Sichuan, China, in 1983. He received the B.S. degree from the University of Electronic Science and Technology of China, Chengdu, China, in 2005, and the Ph.D. degree without going through the conventional master's degree from Southeast University, Nanjing, China, in 2010.

Since 2010, he has been with the School of Electronic Science and Engineering, University of Electronic Science and Technology of China, where he is currently a Professor. From 2012 to 2013, he was a member of Research Staff with the Department of Electrical and Computer Engineering, National University of Singapore, Singapore. He has authored or co-authored more than 100 papers in journals and conferences, and a book *Substrate Integrated Antennas and Arrays* (CRC Press, 2015). His current research interests include microwave and millimeter-wave antennas, arrays, and circuits.

Dr. Cheng was the recipient of the National Science Fund for Excellent Young Scholars in 2016, the Chang Jiang Scholars Program (Young Scholars) in 2016, the National Program for Support of Top-Notch Young Professionals in 2014, the New Century Excellent Talents in University in 2013, and the National Excellent Doctorate Dissertation of China in 2012. He is currently the Secretary of the joint IEEE Chapters of APS/EMCS, Chengdu, China. He is currently a Senior Member of the Chinese Institute of Electronics. He serves as an Associate Editor for IEEE ANTENNAS AND WIRELESS PROPAGATION LETTERS and on review boards of various technical journals.